Materials and Design 77 (2015) 50–58

Contents lists available at ScienceDirect

Materials and Design

journal homepage: www.elsevier.com/locate/matdes

Fusion weldability studies in aerospace AA7075-T651 using high-power continuous wave laser beam techniques

O.T. Ola *, F.E. Doern

School of Transportation, Aviation and Manufacturing, Red River College of Applied Arts, Science and Technology, 2055 Notre Dame Ave., Winnipeg, MB R3H 0J9, Canada

ARTICLE INFO

Article history:
Received 24 October 2014
Revised 6 March 2015
Accepted 29 March 2015
Available online 30 March 2015

Keywords:
AA7075
Laser beam
Porosity
HAZ liquation cracking
Keyhole
Microstructure

ABSTRACT

The weldability of AA7075-T651 during keyhole laser and laser–arc hybrid welding was studied using microstructural and X-ray radiography techniques. The results showed that the application of cold wire laser welding reduced macroporosity, while the problem of heat-affected zone (HAZ) cracking was appreciably minimized by modifying the amount of heat in the HAZ. It was also found that the welding condition that minimized macroporosity was found unfavorable for resistance to HAZ cracking and vice versa. A compromise between these competing weld discontinuities was realized by a combination of localized modification of the strength of the HAZ and the application of cold wire laser welding. Also, differences were observed in the extent of porosity for Ar-shielded and He-shielded laser welds, where Ar shielding appeared to be more effective in minimizing porosity. In addition, the ability of AA7075-T651 to recover mechanical strength by post-weld natural aging will be useful when post-weld heat treatment is not practicable.

1. Introduction

Precipitation strengthened aluminum alloys play major roles in aerospace structural applications due to their high specific strength (strength-to-weight ratio). AA7075 is an Al–Mg–Zn–Cu precipitation strengthened aluminum alloy that was developed for highly stressed structural aircraft parts and other applications such as bicycle frames. Aircraft structural applications of this alloy include the fabrication of upper wing skins, stringers and horizontal/vertical stabilizers [1] and honeycomb panel frames of supersonic aircrafts [2]. This alloy, in its T6 treatment condition, derives its principal strength from second phase precipitates $MgZn_2$ and MgAlCu particles [3–5]. Analytical study of the strengthening precipitates usually requires the use of high-resolution analytical techniques, such as transmission electron microscopy (TEM), which has been used to determine the isomorphous nature of the phases [4,5]. AA7075 has been considered to be extremely difficult to weld by fusion welding techniques due to its high susceptibility to both solidification cracking in the weld metal and liquation cracking in the heat-affected zone [6–8]. Hu and Richardson related the occurrence of transverse solidification cracking in laser–GMA hybrid welded AA7075-T6 to the influence of arc power and the microstructure of the mushy zone [6]. The presence of solidification and HAZ liquation cracking in gas metal arc welding of the alloy was also related to the solidification structure of the fusion zone by Huang et al. [7]. Also, the observation of HAZ cracking during tungsten inert gas welding of the alloy was attributed to microsegregation of constituents along intergranular regions [8]. In addition to cracking in the weld metal and HAZ, AA7075 is susceptible to macroporosity, which is a common phenomenon in keyhole welding of many aluminum alloys [9–12]. Kim et al. reported on the effect of laser beam characteristics on macroporosity during keyhole laser welding of AA6061 alloy [10]. Also, a study of the feasibility of laser welding of AA7075-T6 showed that the alloy is highly susceptible to porosity [12].

Despite the weldability difficulties encountered during fusion welding of AA7075 and other heat-treatable aluminum alloys, recent developments show continued interest in the application of fusion welding techniques for the joining of aerospace structural aluminum alloys. For example, Airbus recently developed robotic laser welding procedure for joining aluminum stringers to skin materials in some of their aircraft, including the new and very large A380 aircraft, to replace riveted structures [13]. Yang et al. investigated the process, microstructure and mechanical properties of laser welded AA6156-T6 and AA6056-T4 for aircraft fuselage panel applications [14]. In addition, the use of laser–arc hybrid welding for joining precipitation hardened aerospace aluminum alloys such as AA7075 is also becoming increasingly attractive due to the synergistic effect of simultaneously combining a laser beam and

* Corresponding author.
E-mail address: oola@rrc.ca.ca (O.T. Ola).

http://dx.doi.org/10.1016/j.matdes.2015.03.064

an electric arc [6,9]. This synergy that is caused by the interaction of a laser beam and an electric arc in the same process zone on the material usually results in the combination of the advantages of both laser and arc welding. Increased welding speed and weld penetration, improved gap and misalignment tolerance, enhanced process stability and improved overall quality have been reported during laser–arc hybrid welding of various alloys [15–18]. The role of welding wire addition on weld properties is also an important factor, particularly in providing adequate weld reinforcement and mitigating the effect of loss in volatile alloying elements such as Mg and Zn [19].

Although laser and laser–arc hybrid welding appear attractive for joining AA7075 and other aerospace aluminum alloys, a review of literature suggests that information on the weldability of the alloy, especially as it pertains to eliminating the weldability problems encountered during fusion welding of the alloy, is still currently limited. Porosity and cracking appear to be the critical problems limiting the weldability of the alloy, and other precipitation hardened aluminum alloys. However, information on how to avoid or mitigate these problems is scarce in the literature. This present work was carried out to study the weldability of AA7075-T651 during keyhole laser only, laser–arc hybrid and cold wire laser welding with the aim of minimizing or totally eliminating weldability problems in the alloy through proper choice of welding process conditions.

2. Experimental procedure

AA7075-T651 welding coupons, received in the form of plates having dimensions approximately 125 mm × 50 mm × 6.3 mm, and a spool of 0.89 mm diameter $AlSi_5$ (ER4043) welding wire were used in this study. The compositions of the base alloy and the welding wire are presented in Table 1. The surfaces of the welding coupons were ground by using SiC papers and cleaned in acetone in order to remove surface oxides and other possible contaminants, respectively. The welding equipment used consists of a 6 kW continuous wave Y-YAG laser and a Fronius 500 Amp Gas Metal Arc (GMA) welder integrated in the laser–arc hybrid welding configuration using a Yaskawa Motoman HP50 6-axis robot. The equipment was operated in 3 modes, which include laser only welding (without arc or welding wire), laser–arc hybrid welding (with arc and welding wire) and cold wire laser welding (without arc but with cold welding wire). All welds were made as bead-on-plates. The direction of welding relative to the geometry of the welding coupons is shown in Fig. 1. The type of shielding gas, gas flow rate and wire feed speed were varied during welding. The welding parameters used are listed in Table 2. Automated laser pre-heating of some selected samples was carried out before actual welding using parameters in Table 3. The number of preheat passes determined the temperature at the laser interaction spot just before the actual welding, which was measured by a k-type thermocouple attached to Fluke 80TK thermocouple module. The preheating and actual welding were performed automatically within the same welding program. Also, laser only and preheated cold wire laser welds were naturally aged after welding to study the ability of the welded materials to recover mechanical strength without artificial post-weld heat treatment. The procedure for post-weld natural aging (PWNA) involves keeping the as-welded material at room temperature for extended number of days.

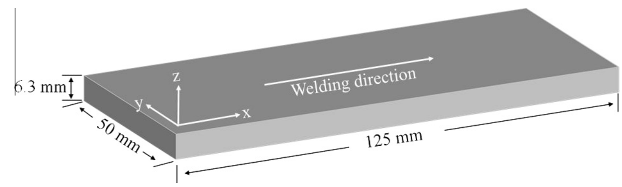

Fig. 1. Welding direction relative to the geometry of the weld coupon.

Table 2
Welding process settings and parameters.

Welding parameters	
Filler wires	ER4043
Wire diameter	0.89 mm (0.035 in)
Laser power	3.5 kW
Laser focus	0 mm (0 in)
Process ordering (hybrid and cold wire laser)	Laser leading
Laser-wire distance (hybrid and cold wire laser)	2 mm (0.079 in)
Welding speed	1.5 m/min (59 in/min)
Wire feed speed	6.5, 8.5, 10.5 m/min (226, 335, 413 in/min)
Shielding gases	Ar, He
Gas flow rate	15, 20 L/min (32, 42 CFH)
Weld type	Bead-on-plate

Table 3
Laser preheat parameters.

Preheat parameters	
Laser power	2 kW
Laser focus	+55 mm (+2.2 in)
Traverse speed	0.6 m/min (23.6 in/min)
Temp. just before welding	260 °C (500 °F)

X-ray radiography of the welded materials was carried out using a VJ Technologies X-ray equipment. The equipment was operated at 130 kV and 5 mA. Radiographs were produced from two planes (*X–Y* and *X–Z*) at right angles to each other parallel to the welding direction. Approximate diameters of pores were determined from the radiographs. The diameters, alongside the dimensions of the weld metal, were used to estimate the percent porosity in the weld metal. The welded coupons were sectioned transverse to the welding direction for microstructural analysis. Ten sections were made from each weld coupon. These sections were prepared by using standard metallographic procedures. In order to reveal the microstructure of the welds, the specimens were chemically etched by immersion in Keller's reagent. They were then analyzed using a Nikkon SMZ800 optical microscope equipped with NIS-Element D imaging software and a Hitachi TM1000 scanning electron microscope (SEM). Analysis of the extent of HAZ cracking was performed using the SEM. The length of individual crack in each of the ten transverse sections was measured. The sum of all crack lengths in the ten sections was determined as the total crack length (TCL). Each welding experiment was repeated two times, making a total of three experiments. The HAZ cracking data for the 3 experiments was finally expressed as average total crack length (ATCL) and standard errors were estimated from the data. In order to

Table 1
Chemical compositions of the base alloy and the welding wire (weight percent).

Alloy	Si	Fe	Cu	Mn	Mg	Cr	Ni	Zn	Ti	Al
AA7075	0.07	0.17	1.59	0.05	2.44	0.18	0.01	5.76	0.02	Bal.
ER4043	5.0	0.8	0.3	0.05	0.05	–	–	0.1	0.2	Bal.